AIR ENTRAINMENT IN CURTAIN COATING WITH CARRIER LAYERS

J.O. Marston[a], ***M.J.H. Simmons***[a], ***S.P. Decent***[b] ***and S.P. Kirk***[b]

[a]*Department of Chemical Engineering, University of Birmingham, Edgbaston, Birmingham, U.K.*

[b]*School of Mathematics, University of Birmingham, Edgbaston, Birmingham, U.K.*

Abstract

The onset of air entrainment was studied using a pilot-scale curtain coating facility. The substrate used was a polished rotating stainless steel wheel which was prewetted with a carrier layer of the coating fluid. The facility was operated over ranges of dimensionless parameters which gave regimes observed in commercial coating processes (Reynolds number: $0.6 < Re < 29$; capillary number: $0.19 < Ca < 2.78$). The substrate velocity for the onset of air entrainment was obtained as a function of the curtain flow rate ($1cm^2s^{-1} < Q < 9cm^2s^{-1}$), fluid viscosity ($0.0326Pa.s < \mu < 0.245Pa.s$), curtain height ($0.035m < h < 0.085m$) and carrier layer thickness. For a given fluid, the presence of a carrier layer led to higher maximum substrate velocities at the onset of air entrainment than were observed in previous works on dry substrates. Images obtained of the free surface at the wetting line verified that the substrate velocity for air entrainment is maximised when the contact line is located directly beneath the impinging curtain. Dimensionless analysis shows that data can be correlated in terms of a critical Reynolds number.

1. Introduction

The use of thin films of liquid to coat solid substrates is a highly important process for the production of photographic film and paper, specialist papers for use in inkjet printing and for the creation of protective layers on reactive solid surfaces. A key driver for industries employing these techniques is the need to produce defect-free coatings as rapidly as possible, hence the speed of operation of the coating process needs to be maximised.

In the curtain coating process, a falling thin liquid sheet impinges upon a moving solid substrate; this forms a wetting line where the liquid film displaces air at the solid surface to form the coating layer. A dynamic contact angle (θ_d) is created between the free surface of the liquid and the solid substrate at the wetting line. This phenomenon is an example of dynamic wetting, which remains one of the great unsolved problems in fluid mechanics, due to the creation of singularities when using conventional fluid mechanics models (Dussan, 1979), which may be removed by generalising the classical continuum formulation (Shikhmurzaev, 1996).

The onset of air entrainment, where bubbles of air are drawn into the liquid film at the wetting line, creates an upper limit for the speed of operation of film coating processes and hence it is essential to be able to predict its occurrence for a given coating system. Air entrainment occurs when the dynamic contact angle exceeds θ_{max} ($< 180^0$), which depends on the material properties of the gas-liquid-solid system. Air entrainment can be observed in any film coating process e.g. dip coating (Burley and Kennedy, 1976; Burley and Jolly, 1984; Cohu & Benkreira, 1998b; Blake & Shikhmurzaev, 2002; Benkreira, 2004), roll coating (Wilkinson, 1975; Bolton & Middleman, 1980; Benkreira, 2002; Benkreira, 2005) and curtain coating (Brown, 1961; Blake et al., 1994; Blake et al., 1999; Clarke, 2002; Blake et al., 2004),

Extensive studies have been made for dip coating, where a tape substrate plunges into a tank of liquid (Burley and Kennedy, 1976; Burley and Jolly, 1984; Cohu & Benkreira, 1998b; Blake & Shikhmurzaev, 2002). For smooth substrates, the maximum velocity of the substrate, U_{ae}, was shown to be a function of the viscosity and surface tension ($U_{ae} =$

$f(\mu, \sigma)$, where μ is the viscosity and σ is the surface tension). These parameters may be correlated using, for example, the equation of Burley and Jolly (1984):

$$U_{ae} = 0.395(\frac{\sigma}{\mu})^{0.77} \tag{1}$$

with μ in $mPa.s$ and σ in mN/m. The dynamic contact angle, θ_d, can be correlated in terms of a capillary number, $Ca = \frac{\mu U}{\sigma}$, where U is the substrate velocity. A concise review of some of the empirical relationships for various coating experiments can be found in Benkreira (2004).

Whilst conventional models suggest that the dynamic contact angle, and hence the onset of air entrainment, should be a function only of the material and fluid properties for any given film coating process, Blake et al. (1994) showed that the global hydrodynamics of the flow had a powerful influence upon the dynamic contact angle in curtain coating, leading to the possibility of wetting speeds which are orders of magnitude higher than is possible for dip coating. This effect, termed *hydrodynamic assist*, can maximize coating speeds by alteration of parameters affecting the flow field e.g. the height of the curtain, h, and the liquid flow rate, Q. Angling of the wetting line was also shown to delay the onset of air entrtainment in a slide coating arrangement by Cohu & Benkreira (1998a).

The work reported above considers coating of smooth, dry, chemically homogeneous solid substrates. However, comparatively few studies have been made for cases where the substrate may be prewetted with fluid (Yu et al., 1995; Yamamura et al., 1999; Chen et al. 2004) or roughened (Clarke, 2002; Benkreira, 2004). Yamamura et al. (1999) measured the onset of air entrainment for a liquid jet impinging onto a rotating polished stainless steel wheel using silicone oils and glycerol-water mixtures with fluid viscosities ranging from 0.01 - 3.3 Pa.s. Whilst convention states that the maximum air entrainment velocity is inversely proportional to the fluid viscosity (Wilkinson, 1975; Burley and Kennedy, 1976; Bolton and Middleman, 1980; Burley and Jolly, 1984; Blake et al., 1994; Cohu & Benkreira, 1998a; Cohu & Benkreira, 1998b), they obtained contradictory results for the high viscosity silicone oils used. In their analysis, however, they did not consider the possibility of residual fluid carry over which was an inevitable consequence of their experiments. Pre-wetting of the surface due to the presence of a carrier layer is known to promote higher coating speeds (Dittman et al., 1977; Bermel et al., 2003). Chen et al. (2004) further demonstrated that the shape of the free surface approaching the wetting line (and hence the onset of air entrainment) is dependent upon the thickness of the carrier layer in a dip coating arrangement using pyrex glass tubes pre-wetted with a layer of the coating liquid. The thickness of the carrier layer was classified as 'thick', where the carrier layer had a thickness of $O(10^{-6}m)$ or 'thin', where the carrier layer was only a few molecules thick i.e. of $O(10^{-9} - 10^{-8})m$. For a thick carrier layer in the low Capillary number range, the viscous bending was small, leading to lower values of θ_d, hence implying higher substrate velocities at the onset of air entrainment.

However, none of these works provide a definitive description of the role of the carrier layer in curtain coating over the large ranges of material, fluid and process parameters used in industry: this phenomenon remains poorly understood.

This paper describes a series of curtain coating experiments to determine how the onset of air entrainment and profile of the free surface is influenced by the presence of a carrier layer on the solid substrate. Experiments were performed using a pilot-scale curtain coating facility using aqueous solutions of glycerol with viscosities ranging from $0.0326Pa.s < \mu < 0.245Pa.s$. The influence of curtain flow rate, Q, curtain height, h, and carrier layer thickness, c, were studied.

2. Materials and Methods

A schematic of the pilot-scale curtain coating facility is shown in Fig. 1. The continuous substrate was provided by a rotating stainless steel wheel, with a diameter of $0.45m$ and a width of $0.06m$. The surface was highly polished so that the average surface deviation was $52nm \pm 2nm$ as measured by an Atomic Force Microscope (AFM). The wheel was driven by a 0.55kW motor with inverter feedback control (Eurotherm 690+ series) producing a maximum substrate velocity of $2.3ms^{-1}$.

The fluids used were aqueous solutions of glycerol (Croda, U.K.) and the properties for the fluids used are given in Table 1. The fluid dynamic viscosities were measured using a Contraves Rheomat-30 viscometer equipped with a cup and bob attachment. Surface tensions were measured using a bubble tensiometer (SITA, Germany). Measurements of these properties were made over a range of temperatures enabling the correct values to be used given the temperature of the fluids used within the facility. Due to ambient laboratory conditions, fluid temperatures varied from $19-24^oC$, however the temperature of the fluids used remained constant over the duration of a single experiment.

The fluids were supplied to a four-slot die of width 0.09m (based on a design by *Kodak Ltd, UK*) using a high accuracy gear pump (series 200, Liquiflo, USA). Flow rates were measured by an electromagnetic flow meter (IFM5020K/D, Krohne, Germany). The integrity of the falling curtain was maintained by using copper wires of $1.6mm$ diameter as edge guides.

Visualisation of the free surface at the wetting line was achieved by bending the edge guides forward out of the plane of the curtain, to allow a clear and undistorted view of the wetting line at the centre of the curtain through the ambient air, as shown in Fig. 2. The influence of this curvature on the central region of the curtain was negligible. Images were obtained using a travelling microscope with a maximum possible optical resolution of $1.5\mu m$, although since several pixels were needed to determine the location of the contact point, the maximum resolution could only be claimed conservatively at an order of magnitude higher than this value. A 1280×1024 pixel CCD camera (7800 series, Cohu Inc., USA) and image grabber attached to a personal computer was used to capture the images. Back illumination was provided by a 90W fibre optic light guide placed behind the rear of the curtain.

Removal of the bulk of the liquid film from the solid substrate post coating was performed using two urethane double-v 'squeegee' blades (Perforag Ltd., UK). By changing the tension of the blades, the amount of the residual carrier layer remaining on the wheel could be altered. Estimates of the thickness of the residual carrier layer were produced by placing absorbent material onto the rotating wheel before the coating die for 10 revolutions during the coating process. The carrier layer thickness was deduced from the weight of fluid absorbed and values are given in Table 2. Results for the thickness of the residual film indicate that the thickness is dependent upon viscosity and the wheel speed, but is consistently of the order of $10^{-7}m - 10^{-6}m$. These then fall into the classification of *thick*.

Measurements of the wheel velocity at the onset of air entrainment were made for each of the fluids given in Table 1 at set curtain heights of 35, 65 and 85 mm. The onset of air entrainment was obtained by increasing the substrate (wheel) velocity at constant curtain flow rate until wetting failure and entrainment of air bubbles was observed with the naked eye. Although wetting failure occurs before air entrainment, these two points could not be distinguished in these experiments, as also observed by Cohu & Benkreira (1998b) for dip coating. The procedure was then repeated for a higher value of curtain flow rate until the substrate velocity at the onset of air entrainment was no longer a function of the curtain flow rate. Each experiment was repeated at least three times and the observed variation was less than 3%.

3. Results and discussion

Images of the profiles of the free surface are shown in Fig. 3 for the 0.0839 Pa.s solution over a range of substrate velocities and curtain flow rates. No air entrainment is present at these conditions. Fig. 3(a-d) show the effect of increasing substrate velocity at a fixed curtain flow rate. A pronounced heel is observed in Fig. 3a and the wetting line is upstream of the falling curtain. Under these conditions recirculation of fluid occurs in the heel as described by Blake et al. (1994). As the substrate velocity increases, the wetting line moves progressively towards the falling curtain until it is directly beneath it (Fig. 3c). Increasing the substrate velocity further causes the heel to disappear and the wetting line moves downstream. A similar behaviour is observed if the substrate speed is kept constant and the curtain flow rate is decreased as shown in Fig. 3 (e-h). This behaviour is consistent with previous findings [Blake et al., 1994; Blake et al., 2004; Yamamura et al., 1999].

The points marked on Fig. 4 correspond to the locations of the free surface profiles shown in Fig. 5. All of the locations marked to the left of the air entrainment curve (a, b, d, f, g) represent successful coating. In Fig. 5g, where the wetting line is considerably upstream of the falling curtain, the wetting line becomes isolated from the effects of the curtain flow field. Figs. 5c and 5e, which show images located to the right of the air entrainment curve in Fig. 4, show that air entrainment can occur with or without the formation of a heel.

Fig. 6 demonstrates the effect of both the fluid viscosity and curtain height on the profile of the free surface near the contact line at similar curtain flow rates and substrate velocities. The images in rows (Figs. 6a, 6b; Figs. 6c, 6d; Figs. 6e, 6f) are taken for the same fluid viscosity and the images in columns (Figs. 6a, 6c, 6e; Figs. 6b, 6d, 6f) are taken at constant curtain height. Considering the images in columns in turn, the position of the wetting line moves downstream with increasing viscosity and hence the size of the heel diminishes. This is due to the reduction in the influence of the inertia of the curtain due to viscous effects. For the images in rows, increasing the curtain height causes the wetting line to move upstream, increasing the size of the heel, due to the increase in impingement velocity (and hence inertia) due to the free-fall of the curtain under gravity.

Figs. 7(a-c) show air entrainment data, plotted as curtain flow rate versus substrate velocity for curtain heights of 35mm, 65mm and 85mm respectively. At low curtain flow rates, Fig. 7(a) shows large increases in substrate velocity for marginal increases in curtain flow rate for the $0.0326 Pa.s$ and $0.0839 Pa.s$ solutions and the maximum substrate velocity is observed at a lower curtain flow rate than observed for the $0.245 Pa.s$ solution. Figs. 7(b) and 7(c) also show maximum substrate velocities, which decrease with increasing viscosity. Fig. 7 shows that all the air entrainment curves tend to a substrate velocity which is independent of curtain flow rate at high curtain flow rates, but this is more readily observed for the two higher curtain heights of $65mm$ and $85mm$. This is unsurprising, since, as shown in Fig. 6, increasing curtain height leads to higher inertial effects at the wetting line. The onset of flow field independence occurs at higher curtain flow rates as the viscosity is increased. The maximum substrate velocity observed occurs in all cases when the position of the wetting line is directly beneath the impinging curtain, as observed by Blake (1994). An image of the free surface at the flow rate for which the maximum substrate velocity occurs for the data presented in Fig. 7(b) for the 0.0839 Pa.s solution is given in Fig. 3(g).

The data presented in Fig. 7 is replotted in Fig. 8 for constant curtain height. Fig. 8(a) shows that for the $0.0326 Pa.s$ solution, increasing the height from $35mm$ to $85mm$ leads to an increase of the maximum substrate velocity from $1.25 ms^{-1}$ to $1.66 ms^{-1}$. Similar increases are noted for the $0.0839 Pa.s$ and $0.245 Pa.s$ solutions in Figs. 8 (b) and (c) respectively. A feature common for all the fluid viscosities used is that higher substrate velocities are attainable at lower curtain heights above the maximum substrate velocity. In each of Figs. 8 (a-c), the values of U obtained converge to a single value when the wetting

becomes independent of the flow field (U_i). Once this point is reached, the only forces acting at the wetting line are those due to surface tension and viscosity, which implies the same physical mechanisms witnessed in dip coating. The vertical lines on Figs. 8 (a-c) represent the velocity predicted by Burley and Jolly (1984), given in equation (1). Some discrepancies between the measured values of U_i and the prediction is noted. These are tabulated in Table 3, together with previous data obtained for curtain coating onto a dry substrate (Blake et al., 1999; Blake et al., 2004) and coating onto a pre-wetted surface (Wilkinson, 1975).

The data show that for a dry homogeneous substrate, in the absence of any hydrodynamic assist, the maximum attainable substrate velocities for dip coating and curtain coating should coincide. The data of Wilkinson (1975) and the current data feature a similar discrepancy where the measured values of U_i are much higher than the values predicted by equation (1); the differences are typically $0.15 - 0.20ms^{-1}$. Indeed, the maximum substrate velocity, U_{max}, measured by Blake et al. for a 0.025 Pas solution is lower than the maximum substrate velocity measured for the 0.0326 and 0.0839 Pa.s solutions (taken at a similar curtain height) in this study. It can therefore be postulated that the differences are due to the presence of the carrier layer on the surface of the solid substrate. The carrier layer thicknesses shown in Table 2 fall into the classification of 'thick' made by Chen et al. (2004). The data from Table 2 imply that the carrier layer for the $0.0326Pa.s$ solution is $O(10^{-7}m)$ whilst the carrier layer for the 0.0839 and $0.245Pa.s$ solutions is an order of magnitude higher ($O(10^{-}6m)$). However, higher entrainment velocities are observed regardless of the carrier layer thickness.

Despite the influence of the carrier layer, the role of viscosity upon the degree of hydrodynamic assist is not clear from the current data. Blake et al. (1994) showed that it was possible to produce a 'master' air entrainment curve for fluids of viscosities ranging from $0.063 - 0.22Pa.s$ by plotting the normalized relative wetting line position versus normalized substrate velocity (at the clearing of air entrainment). A similar set of air entrainment curves may be produced by plotting a modified Reynolds number at air entrainment, $Re_m = \frac{\rho Q u_c}{\mu U_{ae}}$ (where $u_c = \sqrt{2gh}$ is the impingement velocity of the curtain), versus normalized substrate velocity ($U' = U/U_{max}$). These curves are presented in Figs. 9 and 10 for fluids where the carrier layers are thick at $O(10^{-7}m)$ and $O(10^{-}6m)$ respectively.

The curves presented in Figs. 9 and 10 follow the same general shape, yet the values of Re_m obtained at $U' = U/U_{max} = 1$ (the maximum substrate velocity), and the value at $U' = U/U_{max} \approx 0.5$ (flow field independence) are different. On Fig. 9, at $U' = 1$, the first critical Reynolds number identified is $Re_c \approx 6$ whilst the value at $U' \approx 0.5$ is $Re_i \approx 20$. The data for the two higher viscosity solutions in Fig. 10 appear to collapse onto a single 'master curve'. In this case, $Re_c \approx 3$ and $Re_i \approx 12$. Whilst these observations may be due to differences in the carrier layer thicknesses, and hence degree of viscous bending at the free surface may be less for thick carrier layers, further work is necessary in order to be able to decouple the influences of fluid viscosity and carrier layer thickness.

4. Conclusions

An experimental study into the effect of carrier layers in curtain coating has been performed. Images of the free surface and the onset of air entrainment have been obtained for fluids of different viscosity over a range of substrate velocities and curtain flow rates. The influences of curtain height and carrier layer thickness have been examined.

Free surface images confirmed previous findings that the maximum coating speed is always attained when the wetting line is beneath the impingement zone of the curtain. For each fluid, as the curtain flow rate is increased, the substrate velocity at the onset of air entrainment eventually becomes independent of the flow field of the curtain and is only

dependent upon the fluid properties (viscosity and surface tension) which allows comparison with correlations produced for dip coating.

A general trend of decreasing maximum substrate velocity at the onset of air entrainment with increasing viscosity is observed, which is in accordance with previous works. However, a remarkable difference was noted when compared with previous work on dip coating and curtain coating onto smooth, dry substrates. These differences are proposed to be due to the presence of a carrier layer. Dimensionless curves presented in the form of a modified Reynolds number versus normalized substrate velocity for thin and thick carrier layers follow the same general trend, although differences in the values of Re_c at the maximum substrate and the value of Re_i at the onset of flow field independence could be explained by a combined effect of both viscosity and carrier layer thickness. Further work is necessary in order to decouple these two effects, by performing experiments onto carrier layers of different thicknesses for fluids of the same viscosity.

References

[1] Bermel, M.S., McKeown, S.P. & Ruschak, K.J. 2003 Slide bead coating with a low viscosity carrier layer. US Patent 6,579,569.

[2] Benkreira, H. 2002 Experimental study of dynamic wetting in reverse-roll coating *AIChE J.* **48**, (2), 221 – 226.

[3] Benkreira, H. 2004 The effect of substrate roughness on air entrainment in dip coating *Chem Eng Sci.* **59**, 2745 – 2751.

[4] Benkreira, H. 2005 Dynamic wetting in metering and pre-metered forward roll coating. Submitted to *Chem Eng Sci.*.

[5] Blake, T.D., Clarke, A. & Ruschak, K.J. 1994 hydrodynamic assist of dynamic wetting *AIChE J.*, **40**,(2), 229 – 242.

[6] Blake, T.D., Bracke, M. & Shikhmurzaev, Y.D. 1999 Experimental evidence of nonlocal hydrodynamic influence on the dynamic contact angle *Phys. Fluids* **11**, 1995 – 2007.

[7] Blake, T.D. & Shikhmurzaev, Y.D. 2002 Dynamic wetting by liquids of different viscosity. *J. Colloid interface sci.* **253**, 196 – 202.

[8] Blake, T.D., Dobson, R.A. & Ruschak, K.J. 2004 Wetting at high capillary numbers *J. Colloid and Interface Sci.* **279**, 198 – 205.

[9] Bolton, B. & Middleman, S. 1980 Air entrainment in a roll coating system *Chem Eng Sci.* **35**, 597 – 601.

[10] Brown, D. R. 1961 A study of the behaviour of a thin sheet of moving liquid *J. Fluid Mech.* **10**, 297-305.

[11] Burley, R. & Kennedy, S.B. 1976 An experimental study of air entrainment at a solid/liquid/gas interface *Chem Eng Sci.*, **31**, 901 – 911.

[12] Burley, R. & Jolly, R.P.S. 1983 Entrainment of air into liquids by a high speed continuous solid surface *Chem Eng Sci.*, **39**, 1357 – 1372.

[13] Chen, X., Rame, E. & Garoff, S. 2004 The effects of thin and ultrathin liquid films on dynamic wetting *Phys. Fluids*, **16**,(2), 287 – 297.

[14] Clarke, A. 2002 Coating on a rough surface *AIChE J.* **48**, 2149 – 2156.

[15] Cohu, O. & Benkraira, H. 1998a Angling the wetting line retards air entrainment in premetered coating flows *AIChE J.* **44**,(5), 1207 – 1209.

[16] Cohu, O. & Benkraira, H. 1998b Entrainment of air by a solid surface plunging into a non-Newtonian liquid *AIChE J.* **44**,(11), 2360 – 2368.

[17] Decent, S. P. 2005 Hydrodynamic assist and the dynamic contact angle in the coalescence of liquid drops. Submitted to *Int. J. Multi-Phase flow.*.

[18] Dittman, D. A. & Rozzi, A. 1977 Method of multi-layer coating. US Patent 4,001,024.

[19] Dussan V., E.B., 1979 On the spreading of liquids on solid surfaces: static and dynamic contact lines *Ann. Rev. Fluid Mech.* **11**, 371 – 400.

[20] Le Grand, N., Brunet, P., Lebon, L. & Limat, L. 2005 Propagating waves pattern in a falling liquid curtain. Submitted to *J. Fluid Mech.*.

[21] Shikhmurzaev, Y.D. 1996 Dynamic contact angles and flow in vicinity of moving contact line *AIChE J.* **42**,(3), 601-612.

[22] Wilkinson, W.L. 1975 Entrainment of air by a solid surface entering a liquid/air interface *Chem Eng Sci.* **30**, 1227 – 1230.

[23] Yamamura, M., Suematsu, S., Toshihisa, K., Adachi, K. 1999 Experimental investigation of air entrainment in a vertical liquid jet flowing down onto a rotating roll *Chem Eng Sci.* **55**, 931 – 942.

[24] Yu, W., Liu, T. & Yu, T. 1995 Reduction of the minimum wet thickness in extrusion slot coating *Chem Eng Sci.* **50**, (6), 917 – 920.

Fluid	Viscosity ($Pa.s$)	Density (kgm^{-3})	Surface Tension (Nm^{-1})
90% glycerol soln	0.245	1236	0.064
82% glycerol soln	0.0839	1220	0.0659
72% glycerol soln	0.0326	1185	0.0654

Table 1: Properties of glycerol-water mixtures.

Fluid Viscosity ($Pa.s$)	Q (cm^2s^{-1}), U (ms^{-1})	Film Thickness ($\times 10^{-7}m$)
0.0326	2.34, 0.269	1.29
0.0326	2.43, 0.419	1.73
0.0326	2.34, 0.884	2.54
0.0839	2.62, 0.419	6.69
0.0839	2.62, 0.652	12.01
0.0839	3.14, 0.419	11.63
0.245	2.28, 0.419	16.04
0.245	2.28, 0.219	28.94

Table 2: Residual film thickness calculations based on volume of liquid absorbed by material placed on the wheel surface through 10 revolutions.

Data	μ ($mPa.s$)	Coating method	U_{max} (ms^{-1})	U_i (ms^{-1})	U_{bj} (ms^{-1})
Blake '99	25	$3cm$ curtain, dry web	0.8	0.7	0.81
Blake '99	57	$3cm$ curtain, dry web	0.47	0.4	0.43
Blake '04	320	$10.2cm$ curtain, dry web	0.21	0.12	0.115
Wilkinson	245	immersed roll	n/a	0.39	0.14
Fig.7	245	$3.5cm$ curtain, prewet	0.48	0.35	0.14
Fig.7	245	$6.5cm$ curtain, prewet	0.59	0.33	0.14
Fig.7	245	$8.5cm$ curtain, prewet	0.72	0.31	0.14
Fig.7	32.6	$3.5cm$ curtain, prewet	1.25	0.84	0.67
Fig.7	32.6	$6.5cm$ curtain, prewet	1.57	0.84	0.67
Fig.7	32.6	$8.5cm$ curtain, prewet	1.66	0.86	0.67

Table 3: Comparison of air entrainment data. Dry web and prewet refer to the substrate. U_{max} corresponds to the maximum substrate velocity and U_i the velocity which is independent of flow rate. The final column is the velocity predicted by Burley and Jolly for dip coating.

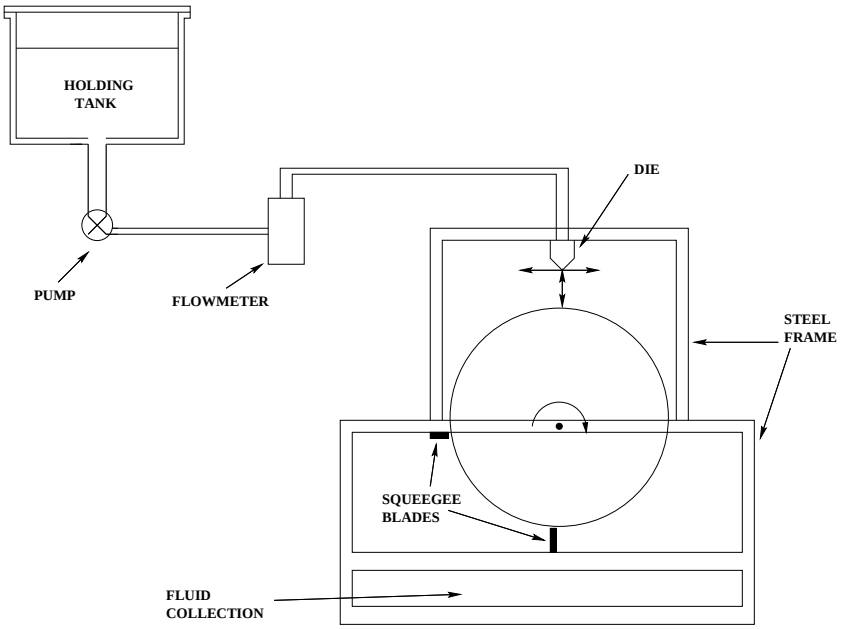

Figure 1: Experimental apparatus.

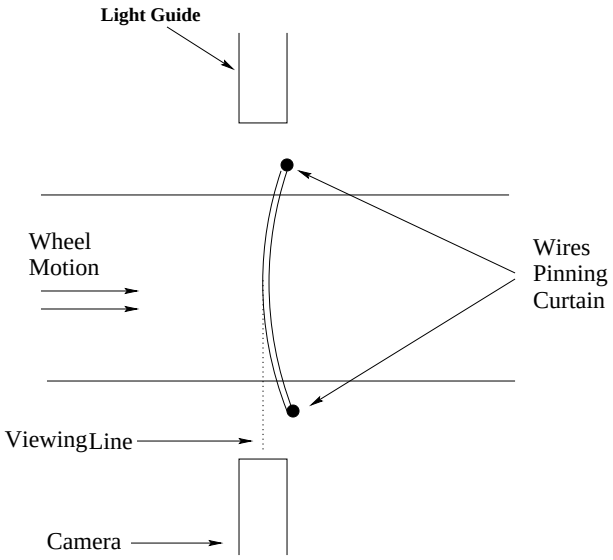

Figure 2: Plan view of the impingement of the curtain.

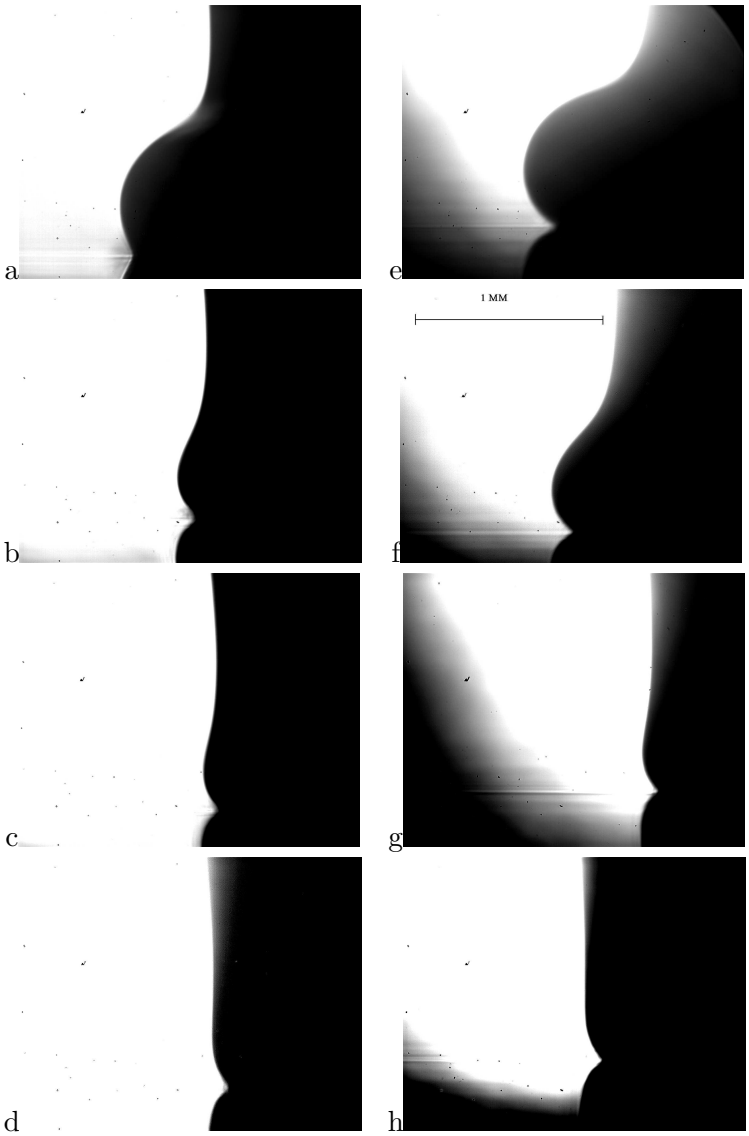

Figure 3: Free surface profiles for the $0.0839 Pa.s$ solution. Images (a)-(d) show the evolution on increasing substrate velocity, U, for a fixed curtain flow rate, Q, of $2.44 cm^2 s^{-1}$ with velocities of 0.22, 0.41, 0.55, $0.88 ms^{-1}$ respectively. Images (e) - (h) show the evolution on decreasing curtain flow rate for $U = 0.83 ms^{-1}$ with $Q = 4.38$, 3.7, 2.81, $2.41 cm^2 s^{-1}$ respectively. Image (f) has a reference length scale that was used for all images.

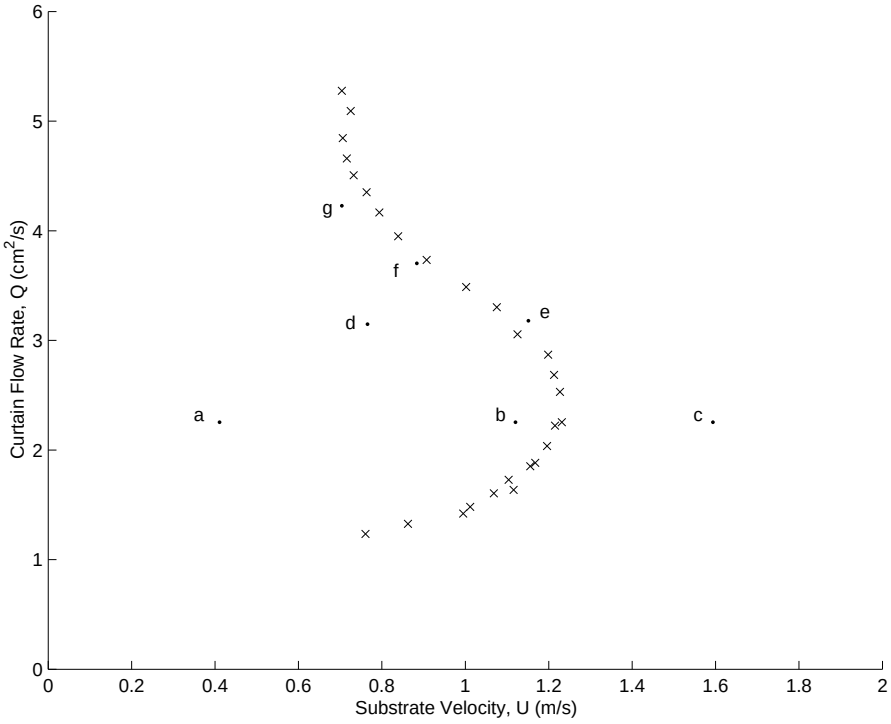

Figure 4: Air entrainment onset curve for $0.0839 Pa.s$ solution with curtain height of $65mm$, with the location of images of the free surface, as given in Fig. 5.

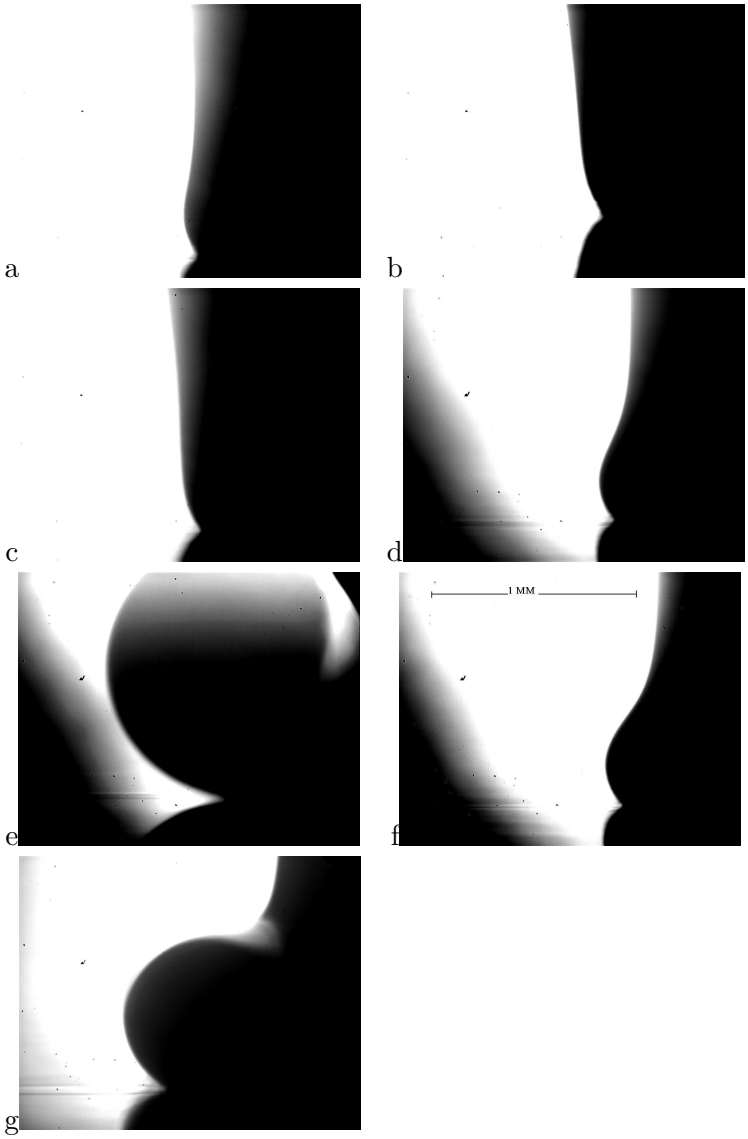

Figure 5: Free surface profiles for the $0.0839 Pa.s$ solution. The images correspond to those located on the air entrainment graph in Fig.4 above. Image (f) has a reference length scale that was used for all images.

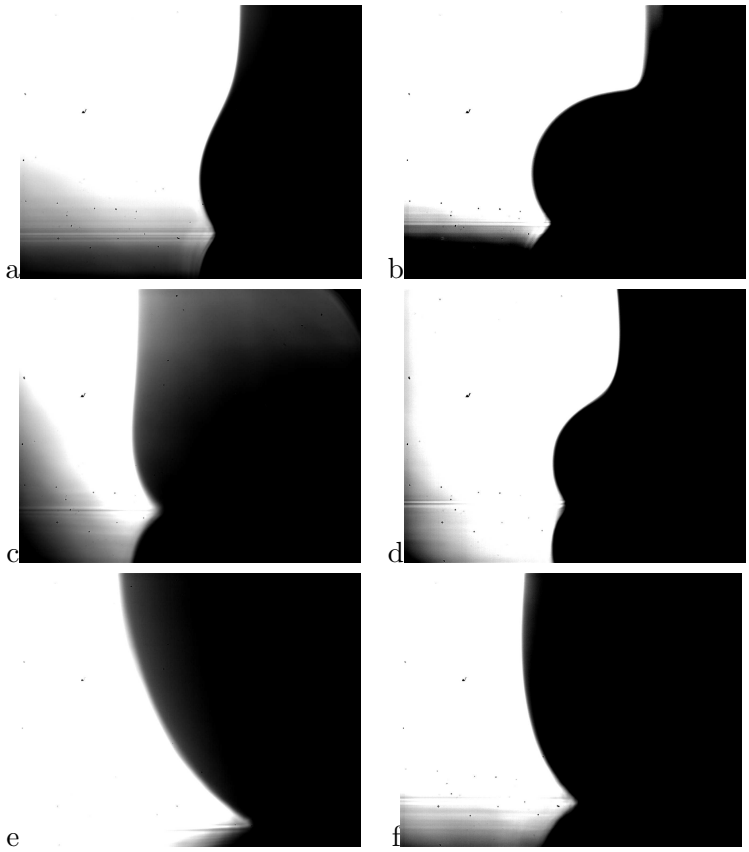

Figure 6: Free surface images for increasing curtain height and viscosity. Images (a) and (b) are for the $0.0326 Pa.s$ solution with substrate velocity, U of $0.27 m/s$ and flow rate,Q of $2.44 cm^2 s^{-1}$. Images (c) and (d) are for the $0.0839 Pa.s$ solution with $U = 0.27 m/s$ and $Q = 2.44 cm^2 s^{-1}$. Images (e) and (f) are for the $0.245 Pa.s$ solution with $U = 0.29 m/s$ and $Q = 2.34 cm^2 s^{-1}$. Images (a), (c) and (e) are for the $35 mm$ curtain height and images (b), (d) and (f) for the $85 mm$ curtain height.

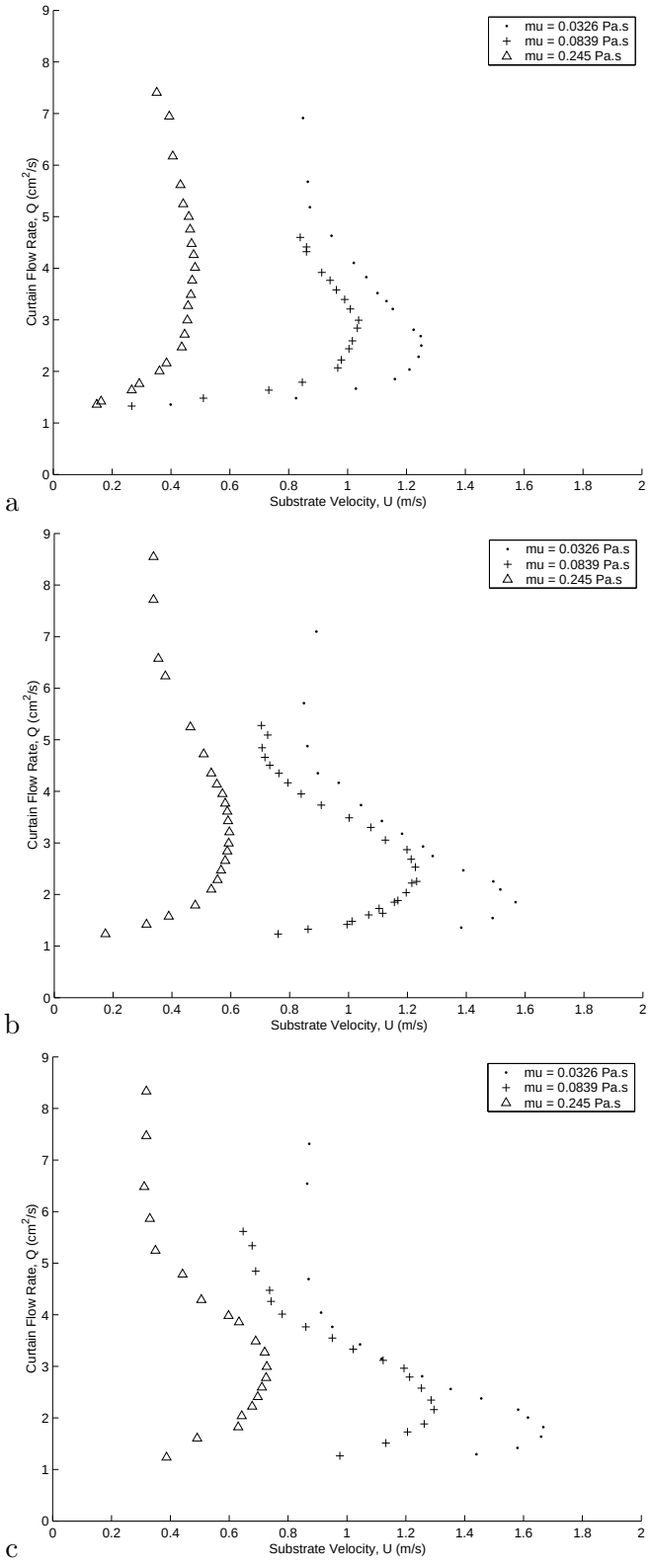

Figure 7: Air entrainment curves for three set heights: (a)35mm, (b)65mm and (c)85mm. The legends indicate viscosity in $mPa.s$.

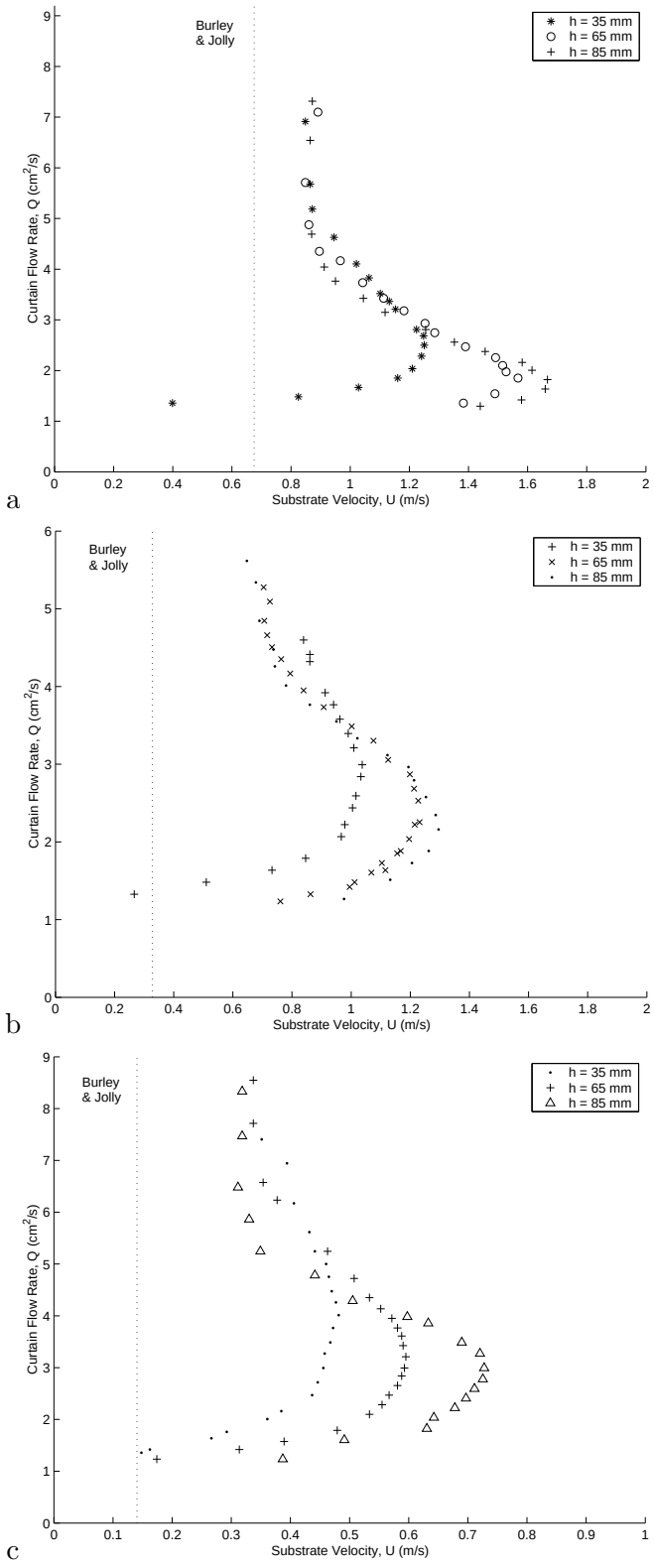

Figure 8: Air entrainment curves for the three viscosities: (a) $0.0326 Pa.s$, (b) $0.0839 Pa.s$ and (c) $0.245 Pa.s$.

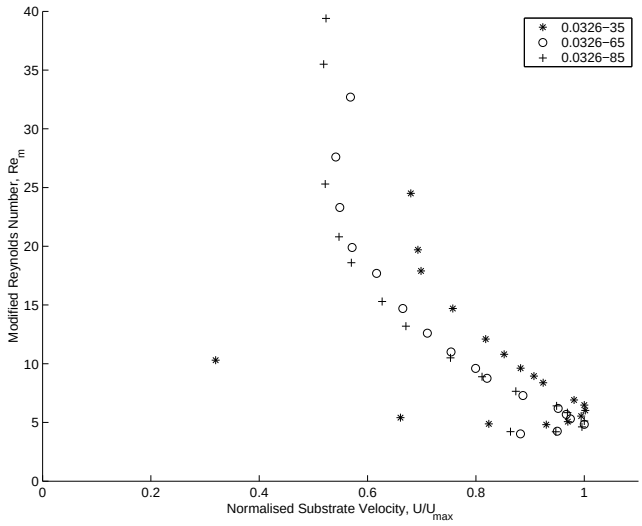

Figure 9: Air entrainment curves for the $0.0326 Pa.s$ solution with a thin carrier layer, plotted as modified Reynolds number against substrate velocity (normalised by the maximum substrate velocity). The legend indicates viscosity ($Pa.s$) and curtain height (mm)

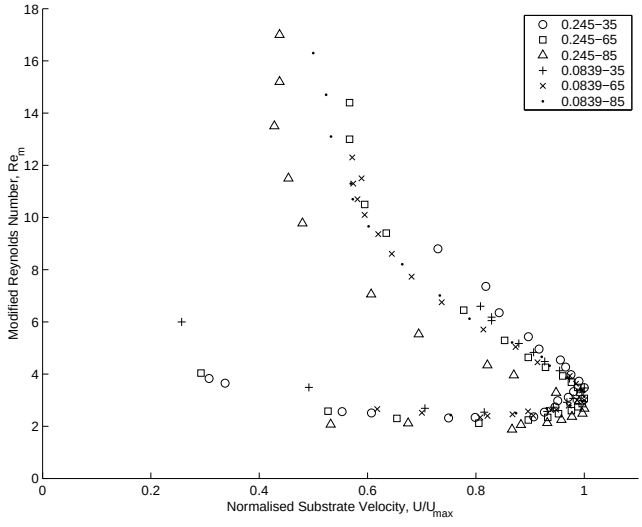

Figure 10: Air entrainment curves for the higher viscosity solutions with thick carrier layers, plotted as modified Reynolds number against substrate velocity (normalised by the maximum substrate velocity). The legend indicates viscosity ($Pa.s$) and curtain height (mm)